catalysts

MDPI

Article

Effect of Zinc on the Structure and Activity of the Cobalt Oxide Catalysts for NO Decomposition

Kateřina Karásková [1,*], Kateřina Pacultová [1], Tereza Bílková [1], Dagmar Fridrichová [1], Martin Koštejn [2], Pavlína Peikertová [3], Paweł Stelmachowski [4], Pavel Kukula [5] and Lucie Obalová [1]

[1] Institute of Environmental Technology, CEET, VSB-Technical University of Ostrava, 17. listopadu 15/2172, 708 00 Ostrava, Czech Republic
[2] Institute of Chemical Process Fundamentals of the CAS, v. v. i., Rozvojová 2/135, 165 02 Prague, Czech Republic
[3] Nanotechnology Centre, CEET, VSB-Technical University of Ostrava, 17. listopadu 15/2172, 708 00 Ostrava, Czech Republic
[4] Faculty of Chemistry, Jagiellonian University, Gronostajowa 2, 30-387 Krakow, Poland
[5] Ranido, s.r.o., Thákurova 531/4, 160 00 Prague, Czech Republic
* Correspondence: katerina.karaskova@vsb.cz

Abstract: $Co_{4-i}Zn_iMnAlO_x$ mixed oxides (i = 0, 0.5 and 1) were prepared by coprecipitation, subsequently modified with potassium (2 or 4 wt.% K), and investigated for direct catalytic NO decomposition, one of the most attractive and challenging NO_x abatement processes. The catalysts were characterised by atomic absorption spectroscopy, powder X-ray diffraction, Raman and infrared spectroscopy, temperature-programmed reduction by hydrogen, the temperature-programmed desorption of CO_2 and NO, X-ray photoelectron spectroscopy, scanning electron microscopy, the work function, and N_2 physisorption. The partial substitution of cobalt increased the specific surface area, decreased the pore sizes, influenced the surface composition, and obtained acid-base properties as a result of the higher availability of medium and strong basic sites. No visible changes in the morphology, crystallite size, and work function were observed upon the cobalt substitution. The conversion of NO increased after the Co substitution, however, the increase in the amount of zinc did not affect the catalytic activity, whereas a higher amount of potassium caused a decrease in the NO conversion. The results obtained, which were predominantly the acid-base characteristics of the catalyst, are in direct correlation with the proposed NO decomposition reaction mechanisms with NO_x^- as the main reaction intermediates.

Keywords: nitric oxide; catalytic decomposition; Co-spinel; Zn bulk promotion

check for updates

Citation: Karásková, K.; Pacultová, K.; Bílková, T.; Fridrichová, D.; Koštejn, M.; Peikertová, P.; Stelmachowski, P.; Kukula, P.; Obalová, L. Effect of Zinc on the Structure and Activity of the Cobalt Oxide Catalysts for NO Decomposition. *Catalysts* **2023**, *13*, 18. https://doi.org/10.3390/catal13010018

Academic Editors: Małgorzata Rutkowska and Lucjan Chmielarz

Received: 5 December 2022
Revised: 15 December 2022
Accepted: 20 December 2022
Published: 23 December 2022

Copyright: © 2022 by the authors. Licensee MDPI, Basel, Switzerland. This article is an open access article distributed under the terms and conditions of the Creative Commons Attribution (CC BY) license (https://creativecommons.org/licenses/by/4.0/).

1. Introduction

Emissions of NO_x (NO and NO_2), especially NO, have a harmful impact on mankind and represent a serious environmental problem, since NO contributes to the formation of acid rains and photochemical smog. NO_x is emitted from the combustion of fossil fuels, where 95 mol.% NO is present in flue gases and from chemical processes (for example, the production of nitric acid). Among the different technologies for the removal of NO_x, such as a selective catalytic reduction (SCR), selective noncatalytic reduction (SNCR), and NO_x storage reduction (NSR), direct catalytic NO decomposition stands out because no reductants such as ammonia or hydrocarbons are required and the products are eco-friendly N_2 and O_2. Nevertheless, it is far from the commercialization stage and the main problem lies in the lack of a suitable catalyst with a high activity, stability, and selectivity [1].

Various catalytic materials have been studied, such as precious metals [2–4], transition metal ion-exchanged zeolites [5–7], perovskites [8,9], and rare earth oxides [10,11]. Among them, the cobalt mixed oxides with a spinel structure represent the promising group of

catalysts due to their good redox properties [12–17]. Previous reports of NO decomposition over Co_3O_4 described it as one of the most promising single-element oxides for the decomposition of NO, albeit with a low activity [13,18].

The catalytic properties of Co_3O_4 can be changed by a bulk and surface promotion [19–21]. The bulk modification of Co_3O_4 was achieved by introducing divalent Mg^{2+}, Zn^{2+}, Ni^{2+} [22–24], or trivalent Al^{3+} and Mn^{3+} cations [25,26]. The activity of these materials for different reactions depends on the degree of substitution of Co^{2+} and Co^{3+} and the degree of the spinel inversion [23]. The surface promotions by alkali metals increased the activity of Co-based mixed oxides for various reactions [27–30]. Alkali metals act as electronic promoters; due to their low ionisation potential, they transfer a charge to the catalyst surface, forming $A^{\delta+}$—$O_{surf}{}^{\delta-}$ surface dipoles (A is an alkali metal) and decreasing the electron work function [31]. For the NO catalytic decomposition, its presence is crucial [14,15,32] since they allow for the formation of surface NO_x species that act as reaction intermediates [33]. The disadvantage is the low thermal stability of alkali metals at the temperatures applied for the decomposition of NO (>600 °C) due to their sublimation [32,34].

Recent works showed that the introduction of Mn and Al in K/Co_3O_4 led to an increase in the specific surface area caused by the presence of Al [25,35] and an improvement in the stability of the alkali promoter due to the presence of Mn [32] which forms potassium manganese oxides [36,37]. A detailed study of the effect of K in Co_4MnAlO_x showed that the highest NO conversion was associated with the optimal K content of 2–4 wt.% [15,32,37–39]. Further work was focused on the bulk promotion of Mg and the preparation of K-promoted $Co_{4-i}Mg_iMnAlO_x$ by substituting toxic and expensive cobalt with cheaper and more nature-friendly magnesium [40]. It was found that it is possible to compensate a certain amount of cobalt with magnesium, and the conversion of NO over these catalysts was even higher. The highest catalytic activity was achieved on mixed oxides with a Mg/Co molar ratio in the range of 0.05–0.33.

Although the bulk Zn promotion of Co spinels has already been reported [19,20,41–43], its effect on the catalytic activity for the decomposition of NO is unknown. Generally, Zn acts as a structural promoter that stabilises the active phase of the catalysts [41]. Zinc ions can occupy the tetrahedral positions [42] or both the tetrahedral and octahedral sites in the spinel's structure [43], and the substitution of Zn induces changes in the structural and magnetic properties, morphology, and cationic distribution. The promotional effect of the successive doping of Zn and K in Co_3O_4 was investigated in [19,20] for the decomposition of N_2O and the introduction of both promoters led to a beneficial effect and structural and morphological stability.

In this work, the particularised study of K/Co_4MnAlO_x with the Zn bulk promotion (Zn/Co molar ratio of 0.33 or 0.14) was carried out. The aim was to find out whether non-environmentally friendly, expensive cobalt can be substituted with other elements than magnesium and to elucidate the activity and stability of these catalysts for a direct NO decomposition. Furthermore, the effect of changing the zinc content while maintaining a constant potassium content, and vice versa, was studied. The results were compared with the non-doped parent K/Co_4MnAlO_x and the mixed oxides K/Co_4MnAlO_x ($K/Co_3MgMnAlO_x$) doped with Mg [40].

2. Results

2.1. Catalyst Characterisation

2.1.1. Chemical Analysis and Texture

The results of the chemical analysis and the texture of the prepared catalysts are summarized in Table 1. The content of the individual chemical elements (Co, Mn, Al, and Zn) was in agreement with the composition set during the catalyst synthesis, as is visible from the Co:Zn(Co,Mg):Mn:Al molar ratio determined from the atomic absorption spectroscopy (AAS). The real potassium content was lower in all the samples compared to the nominal

concentrations (2 or 4 wt.%) due to the thermal desorption during calcination [34,37] or a non-homogeneous distribution of potassium on the surface.

Table 1. Chemical analysis and texture of prepared mixed oxide catalysts.

Sample	Chemical Analysis [a] (wt.%)					Molar Ratio [b] Co:Zn(Mg):Mn:Al:K	S_{BET} [c] (m^2 g^{-1})	$V_{micro} \cdot 10^3$ (cm^3 g^{-1})	External Surface (m^2 g^{-1})
	Co	Mn	Al	Zn (Mg)	K				
Co3.5Zn0.5MnAl	43.9	11.1	5.4	6.9	0.0	3.5:0.5:0.9:0.9:0.0	57	-	57
2K/Co3.5Zn0.5MnAl	46.5	11.5	5.4	7.1	1.5	3.5:0.5:0.9:0.9:0.2	45	2	39
4K/Co3.5Zn0.5MnAl	41.8	11.0	5.3	6.8	3.0	3.5:0.5:1.0:1.0:0.4	43	3	35
Co3ZnMnAl	39.9	11.4	5.6	14.5	0.0	3.0:1.0:0.9:0.9:0.0	56	-	56
2K/Co3ZnMnAl	39.6	11.6	5.8	14.5	1.4	3.0:1.0:0.9:1.0:0.2	45	3	37
4K/Co3ZnMnAl	39.6	10.7	5.5	14.1	2.6	3.0:1.0:0.9:0.9:0.3	41	3	33
2K/Co3MgMnAl [d]	42.0	12.5	6.7	5.3	1.5	3.0:0.9:1.0:1.0:0.2	47	3	39
2K/Co4MnAl [e]	50.5	12.0	6.0	0.0	1.9	4.0:0.0:1.0:1.0:0.2	39	2	33

[a] Relative experimental error: Co ± 9%, Mn ± 9%, Al ± 11%, Zn ± 11%, Mg ± 5%, K ± 15% (AAS). [b] Calculated based on AAS results. [c] Relative experimental error: ± 5%. [d] Reference sample 2K/Mg1 [40]. [e] Reference sample 2K/Mg0 [40].

The specific surface area of the prepared samples ranged from 39 to 57 m^2 g^{-1}. A decrease in the specific surface area and external surface (S_{BET} minus S_{micro}) was observed with an increase in the potassium content in the Zn-modified samples. Noticeably, a change was observed between the catalysts without potassium and those containing potassium. The samples without potassium did not contain any micropores. The deposition of K caused a decrease in the external surface area and micropore formation by partial pore blocking.

The incorporation of Mg and Zn into the spinel structure resulted in an increase in the specific surface area compared to the parent sample 2K/Co4MnAl. The specific surface area increased in the order of 2K/Co4MnAl < 2KCo3.5Zn0.5MnAl $\leq$ 2K/Co3ZnMnAl < 2K/Co3MgMnAl. The lowest specific surface for the zinc substituted samples had the catalyst with the highest K content.

The pore size distribution profiles for the catalysts with different amounts of zinc and potassium are shown in Figure S1. The curve shapes are similar for all samples and no significant changes in the pore size distribution were observed with the modification of cobalt mixed oxide with different amounts of zinc and potassium. The comparison between the 2K/Co3ZnMnAl, the reference samples 2K/Co3MgMnAl, and the 2K/Co4MnAl catalysts is shown in Figure 1. All catalysts showed s unimodal pore size distribution: for cobalt mixed oxide modified by Mg and Zn (2K/Co3MgMnAl and 2K/Co3ZnMnAl), the maximum was around 38 and 60 nm, respectively. For the reference 2K/Co4MnAl sample, the maximum pore size was larger, around 90 nm, and this sample contained a higher number of larger pores. The trend corresponds well to the lowest surface area of this catalyst.

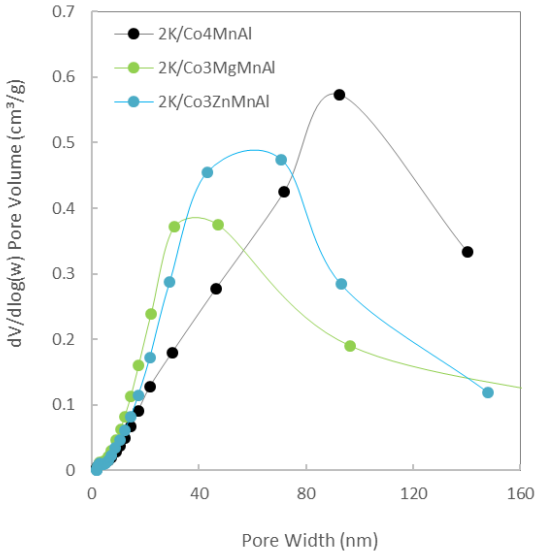

Figure 1. Pore size distribution evaluated from the physical adsorption of nitrogen.

2.1.2. Phase Composition, Raman, and Infrared Spectroscopy

The XRD patterns of the catalysts precursors are shown in Figure S2. Layered double hydroxide (LDH) $Co_{4.8}Zn_{1.8}Al_2(OH)_{10}(CO_3)\cdot 4\ H_2O$ (PDF-2 card no. 00-051-0044) was detected as a major phase. Additionally, minor phases $MnCO_3$ (PDF-2 card no. 00-044-1472) and the spinel Co_3O_4 (PDF-2 card no. 00-043-1003) were detected.

The XRD patterns of all the prepared catalysts are shown in Figure 2. In all samples, the peaks corresponding to crystallographic planes (1 1 1), (2 2 0), (3 1 1), (4 0 0), (4 2 2), (5 1 1), (4 4 0), (5 3 1), (6 2 0), (5 3 3), and (4 4 4) typical for the Co_3O_4 spinel-like phase (S) were found (PDF-2 card no. 01-073-1701). However, this diffraction line can also be ascribed to a different spinel with various substituted cations in the spinel's structure, e.g., $ZnAl_2O_4$, $CoAl_2O_4$, or $MnAl_2O_4$. Unfortunately, it is not possible to determine the exact cationic composition of the spinels on the basis of the measured data. ZnO was not observed in any of the sample, but the $ZnMn_2O_4$ spinel phase (PDF-2 card no. 01-078-4751) can probably be found in potassium-free catalysts (Co3ZnMnAl and Co3.5Zn0.5MnAl). Its main diffraction line (42.2°) overlaps with the main diffraction line of the Co_3O_4 spinel-like phase (43.1°) and the line around 38° corresponds to the overlap of the $ZnMn_2O_4$ phase and the β-line of the main Co_3O_4 spinel-like diffraction line. In articles [37,40], this diffraction line was also attributed to the Mn_2O_3 phase (PDF-2 card no. 01-071-0636). Due to the similar ionic radius of Zn^{2+} (0.60 Å) and Co^{2+} (0.58 Å) [44], the substitution of tetrahedral Co^{2+} by Zn^{2+} is expected in the spinel lattice rather than the Zn segregation as another phase. For potassium-containing catalysts, the potassium manganese oxide phase at 2θ of 14°, 30°, and 50° was determined as $K_{1.39}Mn_3O_6$ (PDF-2 card no. 01-080-7317). This finding agrees with other works in which the K-Mn-O phase was observed [37,45–47].

The cell parameters are comparable for all samples modified with zinc (Table S1). The reference sample 2K/Co4MnAl had the same value of the cell parameter; however, the sample Co4MnAl without potassium (0.822 nm) [40] as well as the reference sample 2K/Co3MgMnAl had higher values of the cell parameters (Table S1). Zinc did not significantly affect the size of crystallite L_c, similarly to the effect reported in [41]. Additionally, crystallite L_c was comparable for both of the reference samples. The detailed characterization of the reference samples 2K/Co3MgMnAl and 2K/Co4MnAl can be found in [40].

The XRD phase analysis was supported by complementary Raman spectroscopy, which is more sensitive to the local structure and the presence of possible minority phases. Raman spectroscopy was performed for 2K/Co4MnAl, 2K/Co3ZnMnAl, 2K/Co3MgMnAl, and Co3ZnMnAl mixed oxides (Figure 3). Each spectrum was created as an average from five dif-

ferent points. The band positions of all curves do not differ more than 3 cm^{-1}; therefore, when the resolution is 4 cm^{-1}, this is not a significant change. The typical bands for the spinel's structure, located at 189 (F_{2g}), 477 (E_g), 515, 615 (F2g), and 680 (A_{1g}) cm $^{-1}$ [48], were observed in all the measured samples (Figure 3), confirming the presence of a nanocrystalline spinel [34]. The observed asymmetry of the Raman peaks and their changes compared to the published values for Co_3O_4: 193–194 (F_{2g}), 479–488 (E_g), 519–522, 617–618 (F_{2g}), and 687–691 (A_{1g}) cm^{-1} result from the substitution of manganese, aluminium, and zinc in the structure of Co_3O_4 [25,49]. The K-Mn-O phase detected by XRD cannot be distinguished in Raman spectra (strong intensity band at 654 cm^{-1}, medium intensity bands at 481 and 581 cm^{-1}, and weak bands at 266 and 170 cm^{-1} [47]) due to an overlap with the spinel bands. The spectrum of 2K/Co3MgMnAl has sharper features, which is clearly visible for the band at 665 cm^{-1}, which could be connected with the better chemical and physical homogeneity [48] of the sample.

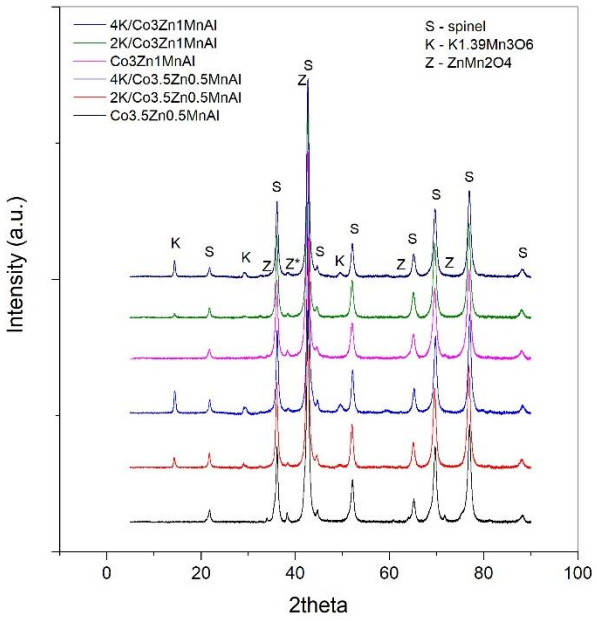

Figure 2. XRD patterns of mixed oxide catalysts, * overlap with spinel β-line.

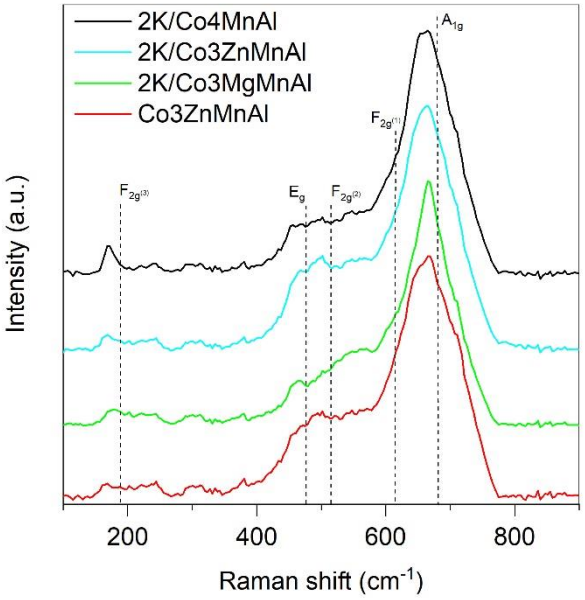

Figure 3. Raman spectra of mixed oxide catalysts. Raman bands position according to [48].

FTIR spectroscopy was used to obtain further information on the potassium form in the prepared catalysts (Figure 4). The observed peak at 1385 cm^{-1} corresponded to ionic potassium species (K-O_{surf}) or K_2CO_{3surf} after the interaction with ambient CO_2 during the IR analysis. The peak at 1407 cm^{-1} was ascribed to potassium cobaltate (K_xCoO_2) or manganate [34]. Although a peak at approximately 1385 cm^{-1} was observed for all of the samples tested, a peak at 1400 cm^{-1} appeared only for the mixed oxide catalysts modified with Mg and Zn. It means that the presence of Zn and Mg enabled a solid-state reaction between the surface potassium and spinel. The confirmation of K_xCoO_2 by Raman spectroscopy was not possible, since broad peaks of oxygen atoms in the CoO_6 octahedra at 469 and 581 cm^{-1} present in K_xCoO_2 [50] cannot be distinguished because they overlap with the spinel bands.

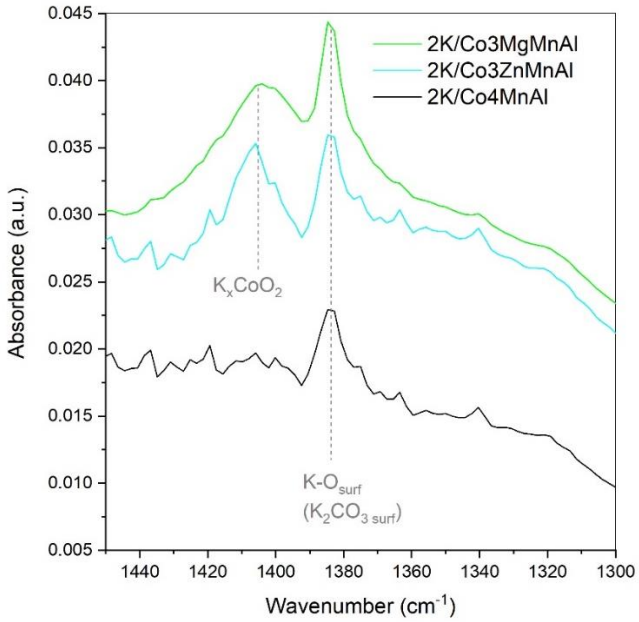

Figure 4. Infrared spectra of prepared mixed oxide catalysts (selected region).

2.1.3. Surface Composition

The surface composition of the 2K/Co3ZnMnAl and 2K/Co4MnAl mixed oxide catalysts was determined by X-ray photoelectron spectroscopy (XPS) and the results were subsequently compared with the published XPS data for 2K/Co3MgMnAl mixed oxide [51] (Table S2). In addition to the main components (Co, Mn, Al, Mg, Zn, O, and K), residual Na was also observed due to an imperfect washing during LDH synthesis.

The deconvoluted XPS spectra of the individual catalyst elements showed similar characteristics that point to the presence of the same components on the surface of all of the catalysts (Figure S3). The binding energies (BE) of the main Co 2p, Mn 2p, and Al 2p peaks used for the determination of the oxidation states are summarised in Table 2.

Table 2. Binding energies (±0.2 eV) of Co $2p_{3/2}$, Mn $2p_{3/2}$, and Al 2p peaks for 2K/Co4MnAl, 2K/Co3ZnMnAl, and 2K/Co3MgMnAl catalysts.

Sample	Co $2p_{3/2}$ (eV)			Mn $2p_{3/2}$ (eV)		Al 2p (eV)
	I. Peak (Co^{3+})	II. Peak (Co^{2+})	III. Peak (Co^{2+})	I. Peak (Mn^{3+})	II. Peak (Mn^{4+})	
2K/Co4MnAl	779.8	781.3	783.4	641.2	643.1	72.9
2K/Co3MgMnAl *	779.9	781.4	783.5	641.6	643.5	72.9
2K/Co3ZnMnAl	780.1	781.6	783.7	641.2	643.1	72.9

* Reference sample [51].

For all of the samples, in the Co 2p region, there were two main photoemission maxima, Co $2p_{3/2}$ and Co $2p_{1/2}$. The binding energy of Co 2p and the shape of the spectra correspond to Co_3O_4, which is consistent with the results published in [52]. Based on our recent XPS study using appropriate standards [53–55] and work [52,56], the lower BE component (around 780 eV) was assigned to octahedral Co^{3+} and the higher BE components (around 781.5 and around 783.5 eV) to tetrahedral Co^{2+}. The positions of the second and third fitting peaks from the first fitting peak were set to +1.5 and +3.6 eV, respectively.

The manganese Mn $2p_{3/2}$ spectra showed a broad peak with a maximum at 641.2–641.6 eV, indicating the presence of oxidation states higher than Mn^{3+}, and this BE corresponds to mixed Mn_2O_3 and MnO_2 [57]. The oxidation state of manganese was determined on the basis of our previous research [37,53,58]. Mn $2p_{3/2}$ was fitted by two peaks corresponding to Mn^{3+} (a component with lower BE) and Mn^{4+} (a component with higher BE). The position of the second fitting peak from the first fitting peak was set to +1.9 eV.

The shapes of the aluminium peaks were similar for all samples. However, in the case of 2K/Co3MgMnAl, the Al spectrum is influenced by the Mg KLL line. The peak could be attributed to Al^{3+}, although its location has lower binding energy values compared to the published data for alpha Al_2O_3 [59]. This shift could be caused by the presence of other metals in the spinel's structure.

The oxygen spectra were deconvoluted to two peaks. The first with BE around 530 eV can be attributed to metal oxide (lattice oxygen O^{2-}) and the second around 531 eV corresponds to C=O bonds and/or to the adsorbed surface oxygen bond to metal oxide, such as O^{2-}, O^{-}, or OH species [60–62].

From the results, it is obvious that Mn^{3+} and Co^{3+} on the surface of all the catalysts prevail over Mn^{4+} and Co^{2+}, respectively (Table 3). The content of Co^{2+} decreases at the expense of Co^{3+} due to the substitution of Co with another metal in the line, none < Mg < Zn. The Mn^{3+}/Mn^{4+} ratio seems to be stable, although there is a slight decrease in this ratio and a slight position shift (Table 2) for the 2K/Co3MgMnAl sample.

Table 3. Results of the deconvolution of the Co 2p, Mn 2p, and O 1s peaks from XPS (with standard deviations ± 0.3) for 2K/Co4MnAl, 2K/Co3ZnMnAl, and 2/Co3MgMnAl catalysts.

Sample	O 1s (529.5 eV) Lattice Oxygen [1]	O 1s (531.2 eV) Chemisorbed Oxygen [1]	Co^{2+}/Co^{3+} Molar Ratio	Mn^{3+}/Mn^{4+} Molar Ratio
2K/Co4MnAl [1]	14.4	4.9	0.7	2.7
2K/Co3MgMnAl *	13.4	8.5	0.6	2.4
2K/Co3ZnMnAl	13.9	5.6	0.3	2.8

[1] Values are related to 3 mol of Co. * Reference sample [51].

In Table 3, the amount of oxygen corresponding to different chemicals is evaluated. The amount of oxygen assigned to the metal oxide (lattice oxygen) was similar for all samples. On the other hand, the amount of oxygen which is bound to the catalyst surface (chemisorbed oxygen) is different. The highest amount of this kind of oxygen was observed for the 2K/Co3MgMnAl mixed oxide catalyst.

2.1.4. Scanning Electron Microscopy (SEM)

The morphology of the prepared potassium-promoted cobalt mixed oxides was studied by SEM. The SEM analysis confirmed that there were no obvious changes in the morphology caused by the incorporation of Mg or Zn into the 2K/Co4MnAl mixed oxide (Figure S4). The catalysts consist of small particles with an almost spherical shape that appear in the form of clusters.

The distributions of elements over cobalt mixed oxide catalysts, which were obtained by SEM mapping, are shown in Figure 5. The white dots represent the individual components. Not all elements were evenly distributed in the particles. Co, Mn, and Al are quite homogenous, however, there are visible places where only Al+O, Al+O+Mg or Al+O+Zn

can be observed. The existence of aluminium oxide or spinel could be considered. The impregnated potassium is distributed almost homogeneously and uniformly.

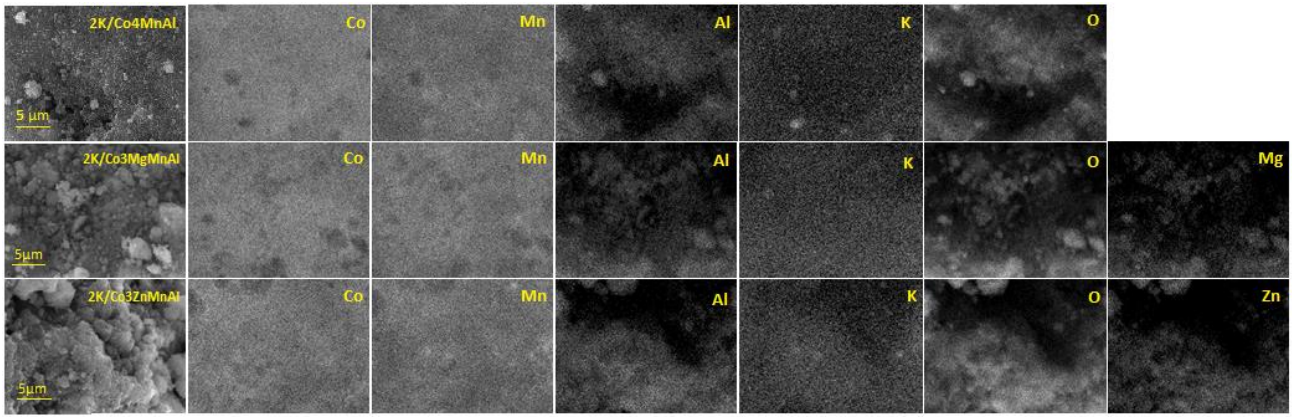

Figure 5. Component dispersal over mixed oxide catalysts from SEM (EDAX).

In Table 4, the chemical composition evaluated by the different methods (AAS, SEM, and XPS) and the surface-to-bulk ratio of the catalyst components are summarised. The results show that the catalyst surface is enriched with potassium and aluminium, in contrast to that of cobalt and zinc. A similar surface enrichment was observed in our previous works [51,53,63]. A surface Al^{3+} segregation was also described by other authors [64]. The higher segregation of Al on the surface of the 2K/Co3MgMnAl catalyst could be due to a different structure confirmed by XRD [40]. The surface and bulk concentrations of Mn and Mg were nearly identical.

Table 4. Representation of individual elements of mixed oxide catalysts obtained by different characterisation techniques.

Scheme	Element	AAS (wt.%)	SEM-EDAX (wt.%)	XPS (wt.%) [a]	Surface-to-Bulk Weight Ratio (XPS/AAS)
2K/Co4MnAl	Co	50.5	60.8	28.7	0.6
	Mn	12.0	15.0	15.2	1.3
	Al	6.0	7.8	10.1	1.7
	O	n.d.	14.3	37.6	-
	K	1.9	2.2	7.7	4.1
2K/Co3MgMnAl	Co	42.0	51.7	20.1	0.5
	Mg	5.3	5.0	5.4	1.0
	Mn	12.5	17.0	12.2	1.0
	Al	6.7	6.8	16.2	2.4
	O	n.d.	17.0	39.7	-
	K	1.5	2.6	5.6	3.7
2K/Co3ZnMnAl	Co	39.6	45.2	19.9	0.5
	Zn	14.5	15.6	11.5	0.8
	Mn	11.6	14.1	14.3	1.2
	Al	5.8	5.9	8.2	1.4
	O	n.d.	17.0	38.9	-
	K	1.4	2.3	9.2	6.6

[a] calculated without carbon tape was used to attach the samples to the holder, which could cause a higher concentration of C.

2.1.5. Reducibility

The reduction of the prepared catalysts was studied by a temperature-programmed reduction (TPR) by hydrogen. The maximum temperature used during TPR-H_2 was 600 °C to avoid an alkali desorption and damage to the temperature conductivity detector. For that reason, only low-temperature peaks, which are relevant from a catalytic point of view, are visible and discussed. The peak maxima and H_2 consumption are shown in Table 5. The H_2 consumption was lower for 2K/Co3MgMnAl and 2K/Co3ZnMnAl compared to 2K/Co4MnAl because the reducible part of Co was substituted with nonreducible

magnesium and zinc. The TPR patterns of the 2K/Co3ZnMnAl catalyst and two reference samples (2K/Co4MnAl and 2K/Co3MgMnAl) are shown in Figure 6.

Table 5. Reducibility of prepared mixed oxide catalysts.

	2K/Co4MnAl [a]	2K/Co3MgMnAl [b]	2K/Co3ZnMnAl
T_{max} from TPR-H_2 (°C) [c]	158; 317; 398	445	155; 389
H_2 consumption at 40–600 °C (mmol g^{-1}) [d]	6.1	5.1	5.4

[a, b]—reference samples, published results in [40]. [c]—experimental error 1.4 %. [d]—experimental error 4.0 %.

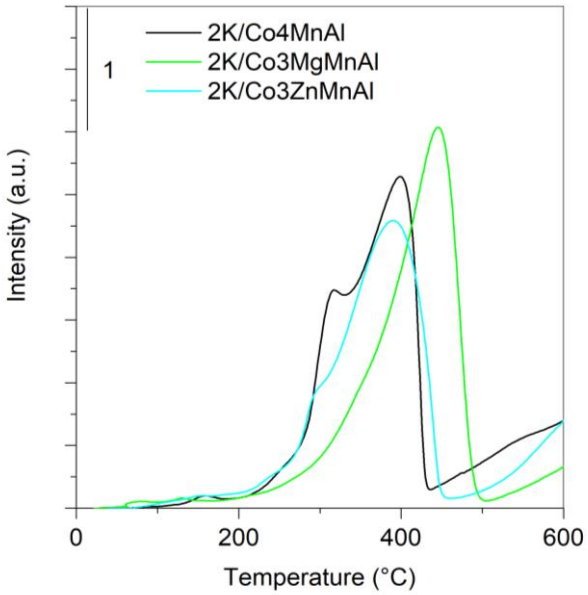

Figure 6. Temperature programmed reduction by H_2.

The TPR profile of the 2K/Co4MnAl reference sample consists of multiple peaks. The first small peak around 158 °C corresponds to the reduction of Co^{4+} or weakly bonded O species [65,66], the next two maxima (the medium temperature range) consist of overlapping peaks corresponding to the co-effect of several reducible species and could represent the reduction of Co^{3+} to Co^{2+} and sequentially to Co^0 in the Co_3O_4-like phase, and the reduction of Mn^{4+} to Mn^{3+} [67]. The reduction of Mn^{3+} to Mn^{2+} can occur in low as well as high (not measured) temperature regions [48].

The medium-temperature peak maximum of the 2K/Co3ZnMnAl catalyst was very similar to that of the 2K/Co4MnAl sample, while a worse reducibility was observed for the 2K/Co3MgMnAl catalyst.

2.1.6. Basicity

The basicity of the catalysts influences the adsorption of the acidic NO molecule [32,68]; this is a significant property of catalysts for direct decomposition of NO [69,70]. The adsorption of NO is a necessary step in the proposed reactions mechanism pathways [71].

The TPD-CO_2 profiles of the 2K/Co3ZnMnAl catalyst and two reference samples (2K/Co4MnAl and 2K/Co3MgMnAl) are shown in Figure 7. Similarly to TPR-H_2, the TPD-CO_2 experiments were also conducted only up to 650 °C to prevent a potassium desorption. The shapes of all the curves are similar; the most different behaviour is obvious for the 2K/Co3MgMnAl catalyst. The first peak is sharp and high and is located at a lower temperature. The contribution of Mg to the increase in the number of weak basic sites was previously confirmed [51]. A high-temperature desorption peak was observed only for potassium-promoted catalysts, not for catalysts without potassium (Figure S5). In the temperature region above 200 °C, the shapes of the signals are similar for all samples. The first two deconvoluted peaks represent weak basic sites. Their temperature maxima were nearly

the same for the 2K/Co4MnAl and 2K/Co3ZnMnAl samples; for the 2K/Co3MgMnAl catalysts a decrease in the T_{max} of these two peaks was observed (Table 6). The peaks above 250 °C were attributed to medium and strong basic sites. The total amount (peaks I.–V.) and amount of medium and strong basic sites (peaks III. + IV. + V.) was nearly the same for 2K/Co4MnAl and 2K/Co3ZnMnAl and increased significantly in the case of the 2K/Co3MgMnAl sample (Table 6). Basic sites with temperature maxima between 250 and 400 °C were previously confirmed as species that play an important role in the catalytic decomposition of NO [37]. These basic sites are predominantly ensured by the presence of potassium, not magnesium or zinc, which is present in a mixed oxide structure.

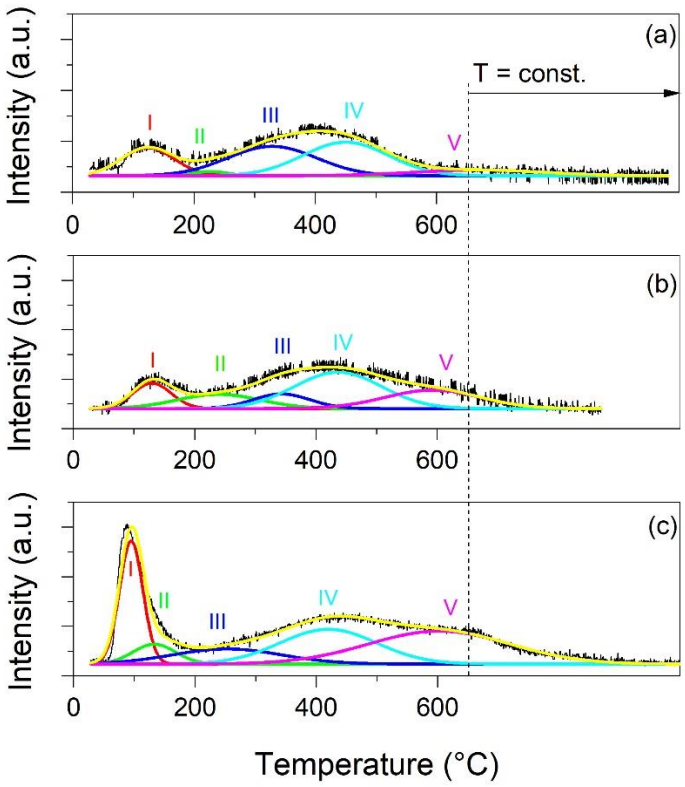

Figure 7. Temperature-programmed desorption of CO_2 (TPD-CO_2) over (**a**) 2K/Co4MnAl; (**b**) 2K/Co3ZnMnAl; and (**c**) 2K/Co3MgMnAl mixed oxide catalysts.

Table 6. Temperature maxima and peak areas obtained from TPD-CO_2 measurements.

Temperature Region		I.	II.	III.	IV.	V.	III. + IV. + V.	Total (I.–V.)
T_{max} (°C)	2K/Co4MnAl	124	226	329	450	>650		
	2K/Co3ZnMnAl	130	240	343	437	593		
	2K/Co3MgMnAl	95	133	253	420	603		
Peak area (a.u.)	2K/Co4MnAl	60	6	106	117	30	253	319
	2K/Co3ZnMnAl	40	49	35	133	74	242	331
	2K/Co3MgMnAl	120	35	68	140	194	402	557

2.1.7. TPD-NO

The temperature-programmed desorption of NO was performed to characterise the various catalyst surface species present during the catalytic process. A detailed study of the evaluation of TPD-NO, including thorough peak deconvolution, was published in [51] where the interpretation of different temperature regions of the desorbed NO and O_2 signals is as follows: temperature regions I, II, and III represent the desorption of loosely bound mononitrosyl species associated with surface M^{3+} in octahedral positions, the dinitrosyl

adducts on Co^{2+} in the tetrahedral position, and the mononitrosyl adspecies on Co^{2+} tetrahedral sites, respectively. The temperature region IV corresponds to the decomposition of the NO_2^- species. Region V represents the desorption of O_2 by the recombination of oxygen atoms that accompany the decomposition of nitrite [51]. In our case, the sample composition is more complex and, except from cobalt species, there could also be Zn^{2+}, Mn^{3+}, a Al^{3+} in the sample. If assumed that the active site is formed by cobalt, the NO and O_2 signals are also divided into five temperature regions (I)–(V). The NO and O_2 signal profiles and their deconvolution are shown in Figure 8. The shapes are similar for all of the investigated catalysts. A small peak of oxygen desorption observed around 250 °C corresponds to weakly bonded oxygen on the surface and is considered to be a spectator species in the NO decomposition reaction [51]. The onset of the main oxygen desorption peak (Figure 8) starts above 320 °C and increases in the line 2K/Co3MgMnAl (320 °C) < 2K/Co3ZnMnAl (326 °C) < 2K/Co4MnAl (356 °C).

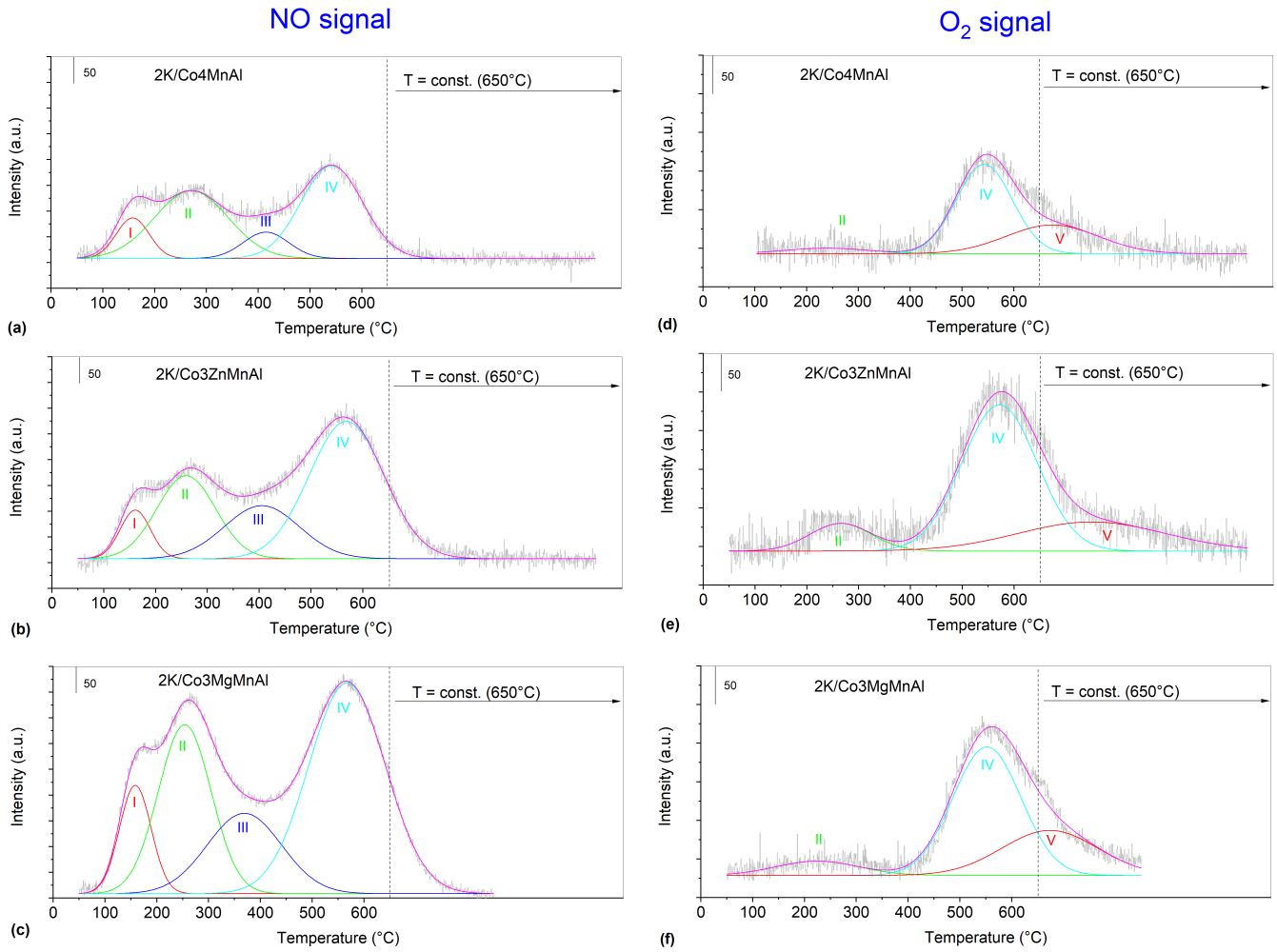

Figure 8. TPD-NO—deconvolution of NO signal for (**a**) 2K/Co4MnAl; (**b**) 2K/Co3ZnMnAl; and (**c**) 2K/Co3MgMnAl mixed oxide and O_2 signals for (**d**) 2K/Co4MnAl; (**e**) 2K/Co3ZnMnAl; and (**f**) 2K/Co3MgMnAl mixed oxide.

Four visible peaks are created by the deconvolution of the NO signals (Figure 8a–c). All deconvoluted peaks are the largest for the 2K/Co3MgMnAl mixed oxide catalyst compared to the other catalysts (Table 7). The increasing amount of adsorbed NO may be connected with an increase in the specific surface area or/and the increasing basicity of the samples. The main desorption peak (peak IV) is developed together with the IV. temperature O_2 desorption peak. It suggests that the formation of the NO_x^- surface intermediates after

the NO adsorption and their decomposition was in the high-temperature range according to [33,51,70,72] since the O_2/NO molar ratio is close to 0.5 (Table 7). In our previous paper [51], it was also discussed that the decrease in the oxygen signal is much slower than the decrease in the NO signal in the isothermal part of the measurement, suggesting that the oxygen peak consists of two different peaks, and the high temperature one (region IV) is responsible for the desorption of oxygen from the surface by the recombination of oxygen atoms. A similar dependence is also observed for the samples presented in this investigation.

Table 7. The temperature maxima of the desorption of NO and O_2 and the peak areas obtained from the TPD-NO measurements.

Experiment/Temperature Region		I.	II.	III.	IV.	V.
T_{max} O_2 (°C)	2K/Co4MnAl		239		543	>650
	2K/Co3ZnMnAl		265		572	>650
	2K/Co3MgMnAl		225		552	>650
T_{max} NO (°C)	2K/Co4MnAl	158	271	415	542	
	2K/Co3ZnMnAl	161	259	405	568	
	2K/Co3MgMnAl	158	254	369	567	
O_2 peak area (a.u.)	2K/Co4MnAl		14		157	83
	2K/Co3ZnMnAl		53		345	134
	2K/Co3MgMnAl		37		274	135
NO peak area (a.u.)	2K/Co4MnAl	63	234	56	270	
	2K/Co3ZnMnAl	69	228	186	484	
	2K/Co3MgMnAl	161	419	281	762	
O_2/NO molar ratio	2K/Co4MnAl		0.1		0.6	
	2K/Co3ZnMnAl		0.2		0.7	
	2K/Co3MgMnAl		0.1		0.4	

During all measurements, not only was the evolution of NO_2 but also the absence of N_2 was observed. This means that the desorption of N_2 during the reaction is fast and N_2 does not accumulate on the catalyst surface during the reaction at 650 °C and even during cooling in the NO/He flow [33,51,73].

2.1.8. Work Function

The catalyst activity in oxidation-reduction reactions was previously found to correlate with the electronic properties of its surface [31,74]. Therefore, the influence of the incorporation of other metals into potassium-promoted cobalt mixed oxide on the changes in the work function (WF) was examined. Potassium, due to its low ionisation potential, transfers a charge to the catalyst and, by the formation of the $K^{\delta+1}$—$Osurf^{\delta-1}$ surface, the dipoles modify the catalyst work function. The lower the work function of the catalyst, the easier the release of oxygen, and thus a correlation of the electronic properties, reactivity, and reducibility can be expected [31].

The measurement of the WF was performed in air at room temperature. Before the measurement of the WF, the studied samples were exposed to air for 5 min at 700 °C in an attempt to simulate the reaction conditions of the decomposition of NO in the oxygen atmosphere. The value of the work function is practically the same for all of the fresh samples, as presented in Table 8. Interestingly, the unchanged work function for the zinc-promoted catalyst contrasts with our previous results, where the addition of zinc caused a decrease in the WF of the materials [19]. However, previously, we used a lower Zn concentration than in the present study, and the increased zinc concentration can modify the bulk electronic structure, resulting in cancelling the promotional effect. For the 2K/Co3ZnMnAl catalyst, no change in the work function was observed for the catalyst used compared to the fresh catalyst, while for the 2K/Co3MgMnAl catalyst, the WF increases. The increase in the WF may be related to the activated adsorption of some

electronegative species or a loss of potassium during the high-temperature pre-treatment. It indicates a higher surface reactivity in the NO decomposition, leading to a more pronounced adsorption at room temperature, increasing the work function of the magnesium-doped catalyst. Therefore, the promotion of Zn may be beneficial for maintaining the catalyst's stability in contrast to the Mg promotion.

Table 8. Work function values.

Sample	WF (Fresh Sample) (eV)	WF (Used Sample) * (eV)
2K/Co4MnAl	4.53 ± 0.01	n.d.
2K/Co3MgMnAl	4.51 ± 0.01	4.62 ± 0.01
2K/Co3ZnMnAl	4.54 ± 0.01	4.53 ± 0.01

* After NO decomposition reaction.

2.2. Catalytic Application—NO Decomposition

The temperature dependence of the NO conversion is shown in Figure 9a. The results of the reference samples 2K/Co3MgMnAl and 2K/Co4MnAl [40] were added for comparison. Co-Zn-Mn-Al mixed oxide catalysts without potassium were not active in the NO decomposition unlike the potassium-promoted samples. The potassium content influenced the catalyst's activity. A higher NO conversion was achieved over the samples modified by 2 wt.% K compared to the catalyst modified by 4 wt.% K. On the contrary, the amount of zinc content (Zn molar content 0.5 or 1) did not influence the final NO conversion. The same trends were observed in the case of the substitution of Co with magnesium [40], where the optimal potassium content was between 1 and 2 wt.% and the substitution of Mg for cobalt in the range of 0.2 to 1 in terms of the molar content did not affect the NO conversion. A partial cobalt substitution in the base 2K/Co4MnAl mixed oxide had a positive effect on the NO conversion and this effect was in the order of Mg > Zn > non-substituted catalyst.

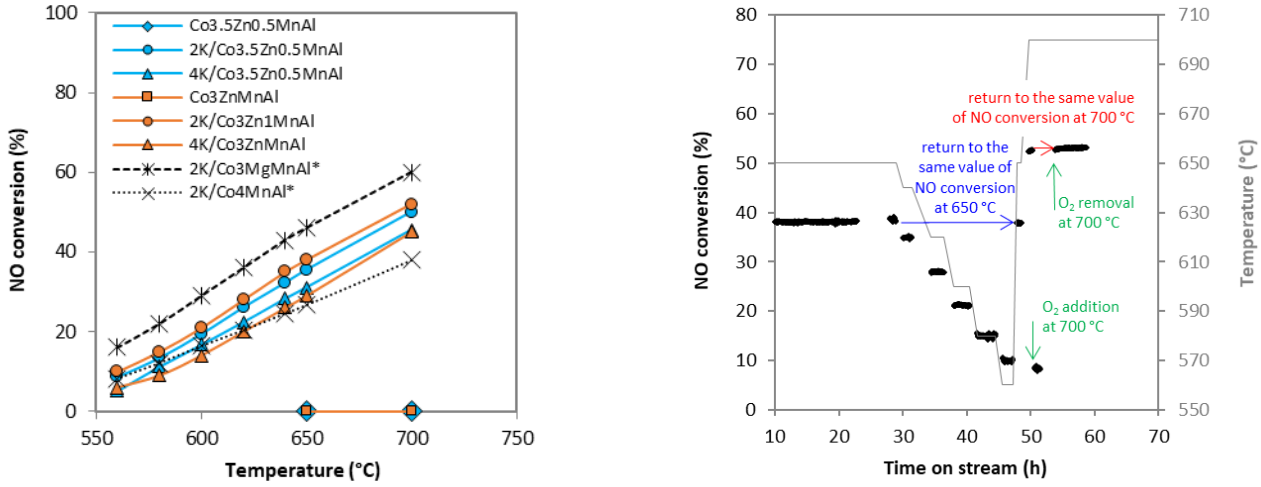

(**a**) (**b**)

Figure 9. Dependence of NO conversion on (**a**) temperature over potassium-promoted mixed oxide catalysts; (**b**) time on stream over 2K/Co3ZnMnAl mixed oxide. Conditions: 0.1 mol.% NO or 0.1 mol.% NO and 2 mol.% O_2 in N_2, WHSV = 6 l g^{-1} h^{-1}, * reference sample [40].

The stability of the prepared catalysts was also verified. The time dependence of a NO conversion over the 2K/Co3ZnMnAl mixed oxide catalyst is shown in Figure 9b. The catalyst was exposed to the reaction conditions for almost 60 h, confirming the stable performance of the catalyst.

All catalysts were also tested for their NO decomposition in an oxygen atmosphere (2 mol.%). The final NO conversion achieved was 5 to 8%, which means a decrease of approximately 84–89% from the original value in an inert atmosphere. The inhibition was reversible; after oxygen was removed from the reaction gas, the initial NO conversion was obtained (Figure 10). In the same trend, a large drop in the NO conversion in the oxygen stream and a return to the same NO conversion was also previously observed for 2K/Co3MgMnAl catalysts [40,51].

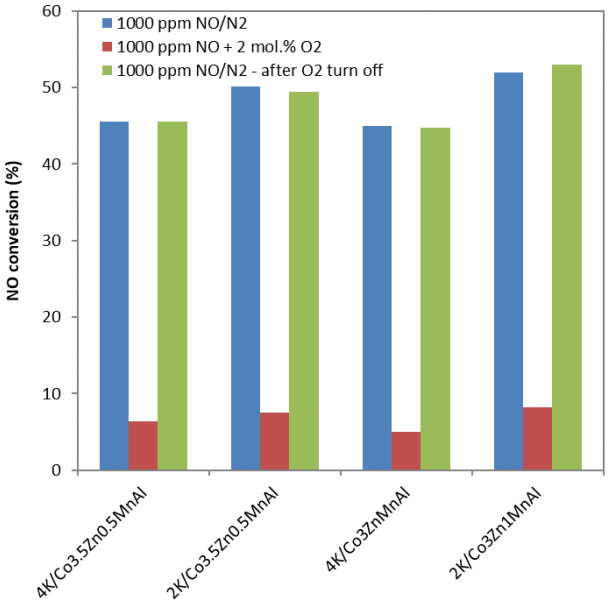

Figure 10. NO conversion over potassium-promoted Co-Zn-Mn-Al mixed oxide catalysts at 700 °C.

3. Discussion

The proposed reaction mechanism of the decomposition of NO over potassium-modified cobalt mixed oxides consists of the following steps [33,51,71]: (i) the chemisorption of NO on transition metals (R1), (ii) the formation of surface intermediates on potassium species (R2), (iii) the desorption of N_2 by a reaction of the intermediates (R3 and R4), (iv) the desorption of O_2 by the reaction of the intermediates (R5 and R6), as well as by an oxygen recombination (R7). Furthermore, the migration of oxygen between the active sites and lattice oxygen vacancy (R8) probably occurs during the decomposition of NO.

$$NO + * \rightarrow NO* \quad (R1)$$

$$NO* + O^{\#} \rightarrow NO_2* + {}^{\#} \quad (R2)$$

$$2.\ NO* \rightarrow N_2 + 2\ O* \quad (R3)$$

$$NO_2* + NO* + {}^{\#} \rightarrow N_2 + O^{\#} + 2\ O* \quad (R4)$$

$$NO_2* \rightarrow NO + O* \quad (R5)$$

$$2.\ NO_2* \rightarrow 2\ NO + O_2 \quad (R6)$$

$$2.\ O* \leftrightarrow O_2 \quad (R7)$$

$$O* + \# \leftrightarrow O\# + * \quad (R8)$$

where * means the active site and # means the oxygen vacancy.

The clear dependence of the NO conversion on the specific surface area is shown in Figure 11. The higher the S_{BET}, the higher the NO conversion over the Co mixed oxide catalyst was. The differences in the surface area were caused by (i) the differences in the specific surface areas of the parent cobalt spinels and (ii) the formation of micropores

connected with the presence of K. The S_{BET} of mixed oxides prepared by the calcination of LDH is dependent on the thermal stability of LDHs guided by their chemical composition (the type and content of the different divalent and trivalent metal cations). The maximum value of the surface area can be achieved in the vicinity of the LDH decomposition temperature. A progressive increase in the calcination temperature leads to the consecutive crystallisation of the arising oxidic phases and a decrease in the surface area. On the other hand, the decomposition of LDH at temperatures much lower than the catalyst calcination temperature showed substantially lower surface areas [75]. Since the presence of Mg in the LDH structure increases its decomposition temperature [35], the S_{BET} of Co3MgMnAl is higher than the mixed oxides of Co4MnAl and CoZnMnAl obtained by the corresponding LDH calcination at 700 °C.

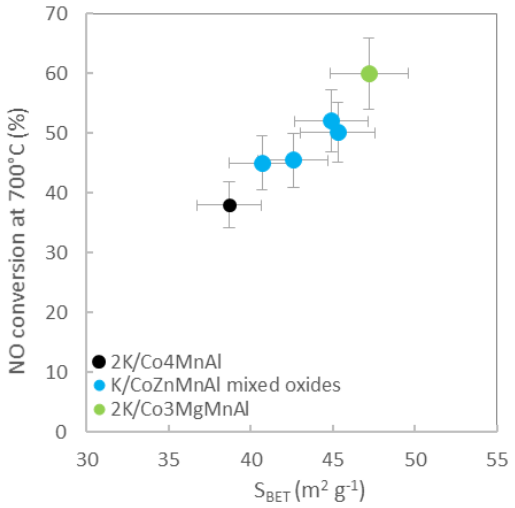

Figure 11. Dependence of NO conversion on the specific surface area.

The higher specific surface area allowed for the accessibility of a higher number of active sites. The achieved NO conversion was found to be higher with a more adsorbed loosely bound mononitrosyl species of NO (the NO peak area of the III. peak in TPD-NO) and also with the surface nitrate (the NO peak area of the IV. peak in TPD-NO) (Figure 12).

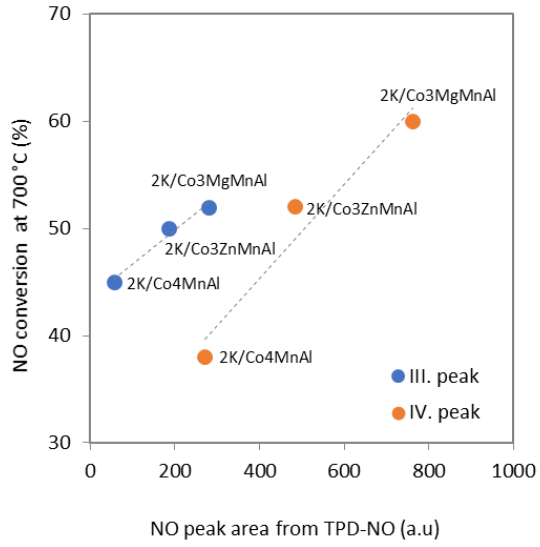

Figure 12. Dependence of NO conversion on NO peak area from TPD-NO.

A direct correlation was found between the activity and the basic properties of the catalysts. On the basis of the results of TPD-CO_2, we could also expect that more NO

should be accumulated on the catalyst with a higher number of basic sites. This assumption was confirmed; the dependence of the amount of desorbed NO on the amount of medium and strong basic sites is seen in Figure 13a. The more basic sites the catalyst has, the greater the amount of NO adsorbed on the catalyst's surface is in accordance with [33,37,55] the surface area of the catalyst (Figure 13b).

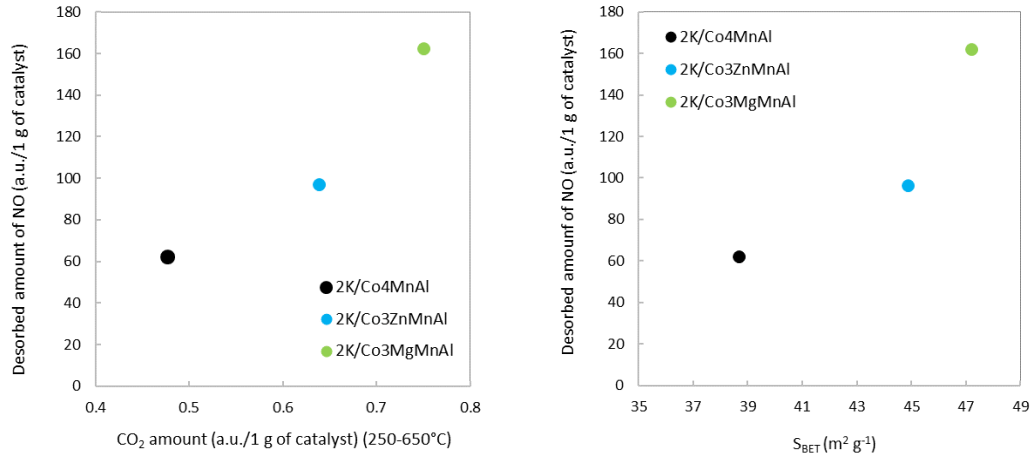

(**a**) (**b**)

Figure 13. Dependence of desorbed NO amount from TPD-NO per weight of catalyst on (**a**) desorbed CO_2 from TPD-CO_2 and (**b**) specific surface area.

The dependence of the conversion of NO on the number of basic sites and the temperature maxima determined from TPD-CO_2 is shown in Figure 14. Consequently, the conversion of NO increased both with an increasing amount of desorbed CO_2 and with a higher temperature maximum of the TPD-CO_2 signal in the line non-modified < Zn modified < Mg modified mixed oxide catalyst.

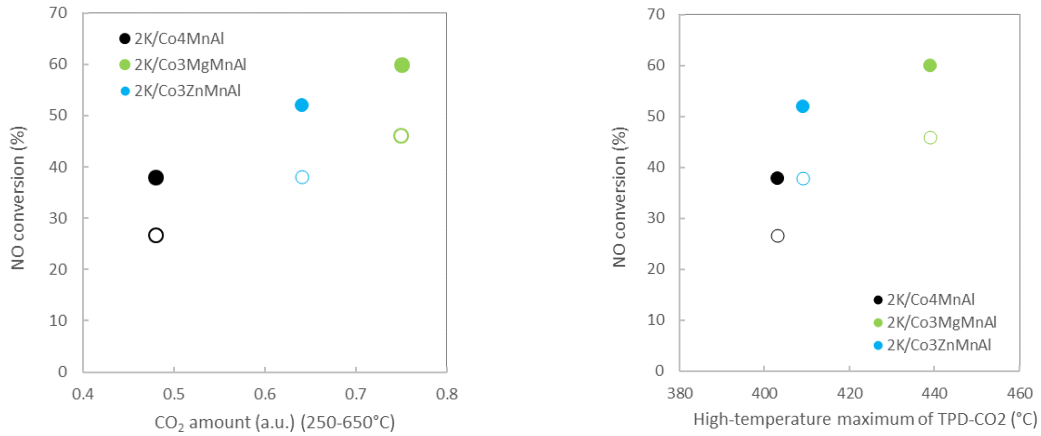

(**a**) (**b**)

Figure 14. The dependence of NO conversion on: (**a**) the number of basic sites; (**b**) high-temperature maximum of TPD-CO_2. Full mark—700 °C, empty mark—650 °C.

The activity of the catalysts also correlates with the amount of lattice and chemisorbed oxygen species determined by XPS (Figure 15). The highest NO conversion was achieved with the 2K/Co3MgMnAl mixed oxide catalyst, which has the highest amount of chemisorbed oxygen and the lowest amount of lattice oxygen species. Oxygen is important for the oxidation of adsorbed NO to NO_2^- intermediates, which can proceed (i) with the surface/subsurface lattice oxygen, when its high mobility corresponding to its low amount

and oxygen vacancies is important, and (ii) with chemisorbed oxygen species, when their high amount is favourable.

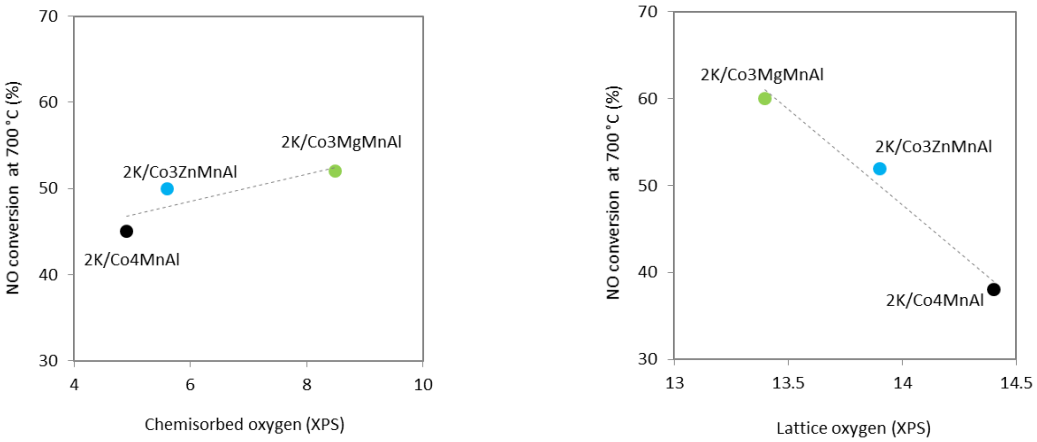

(**a**) (**b**)

Figure 15. Dependence of NO conversion on: (**a**) chemisorbed and (**b**) lattice oxygen.

As a result of the different cobalt content in the samples, the turnover frequency (TOF) was used for the comparison of the activity. The TOF was calculated using the Co amount as the number of active sites since the samples containing manganese instead of cobalt were non-active (unpublished results—manuscript in preparation). The TOF which related to 1 g of cobalt (Table S3) had the same trend as the NO conversion (Figure 16a). Different TOF values indicate that the achieved value of the NO conversion is influenced by the specific surface area and the number of achievable active sites on the catalyst's surface which are associated with it. From the direct correlation between the NO conversion and TOF on the temperature of the O_2 desorption during TPD-NO (Figure 16b), it can be seen that the decisive parameter is also the thermal stability of the reaction intermediates affected by the redox properties given by the chemical composition of the catalysts. Here, the most important is the optimal potassium promoter content, without which the NO decomposition practically does not carry on [15,33,37]. The onset of the desorption of O_2 was observed at the lowest temperature for the most active 2K/Co3MgMnAl mixed oxide catalyst. This finding may indicate that an oxygen desorption through the decomposition of surface nitrite is a crucial step in being in agreement with [33,51,69,71].

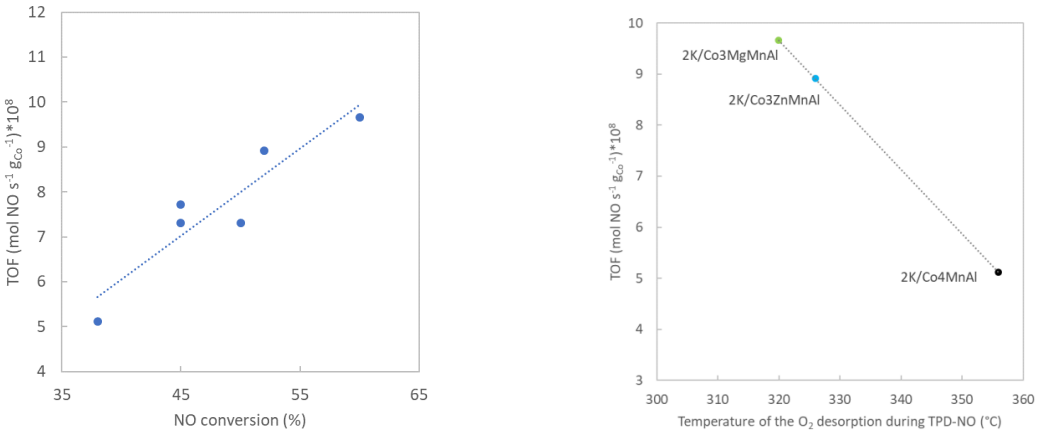

(**a**) (**b**)

Figure 16. Dependence of TOF on: (**a**) NO conversion and (**b**) O_2 desorption.

The crystallite size and cell parameter did not affect the NO conversion. No dependence between the catalysts' reducibility and activity for the NO decomposition was observed (not shown here). Relatively low differences in the work function for the studied materials indicate that the redox properties of the studied catalysts are not the key factor influencing the catalytic activity [37].

Based on the results obtained, the following relationships between the physicochemical and catalytic properties were observed:

- The dependence of the NO conversion on the specific surface area (Figure 11).
- The dependence of the NO conversion on the amount of adsorbed NO species in the form of loosely bound mononitrosyl species and the surface NO_x^- species (Figure 12).
- The dependence of the desorbed amount of NO on the amount of medium and strong basic sites (Figure 13a).
- The dependence of the NO conversion on the number of basic sites and their strength (Figure 14).
- The dependence of the NO conversion on the amount of surface lattice and chemisorbed oxygen species (Figure 15).
- The dependence of the NO conversion and TOF on the temperature of the O_2 desorption during the decomposition of the intermediate KNO_2 surface (Figure 16b).

4. Materials and Methods

4.1. Catalyst Preparation

Co-Zn-Mn-Al layered doubled hydroxide (LDH) precursors with a Co:Zn:Mn:Al molar ratio of 3:1:1:1 and 3.5:0.5:1:1 were prepared by the coprecipitation of the corresponding nitrates (2 litres of solution with 339.4 g or 291 g of $Co(NO_3)_2{\cdot}6\ H_2O$ (Penta, 99% purity), 49.6 g or 99.2 g of $Zn\ (NO_3)_2{\cdot}6\ H_2O$ (Penta, 98% purity), 83.6 g of $Mn(NO_3)_2{\cdot}4\ H_2O$ (Penta, 97% purity), 125 g of $Al(NO_3)_3{\cdot}9\ H_2O$ (Penta, 98% purity)) with Na_2CO_3/NaOH solution (2.4 litres of solution with 242 g Na_2CO_3 (Penta, 99% purity) and 127 g of NaOH (Penta, 98% purity) at 30 °C and pH 10. The washed and dried products were calcined for 4 h at 700 °C in the air. The prepared mixed oxides were crushed and sieved to obtain a fraction with a particle size of 0.016–0.315 mm. The catalysts prepared this way were named Co3ZnMnAl and Co3.5Zn0.5MnAl. The numbers in the name of the catalyst correspond to the initial molar content of the elements in the HT precursor.

In addition, both of the prepared mixed oxides were impregnated using the pore filling method by 0.47 or 0.93 mol/L of the KNO_3 (Penta, 98% purity) water solution. After drying at 105 °C for 4 h, the impregnated samples were calcined at 700 °C for 4 h and sieved to a fraction of 0.016–0.315 mm. The samples were labelled according to their nominal potassium content set during the impregnation procedure, for example, 2K/Co3ZnMnAl means $Co_3ZnMnAlO_x$ mixed oxide modified by 2 wt.% potassium. The x represents the molar content of oxygen, which is unknown but should be close to 8. The amount of potassium (2 and 4 wt.%) was chosen based on the optimal content published in [37,40]. The list of samples is given in Table 1.

To see the effect of the Zn substitution, the catalysts were compared with the reference samples: (i) parent mixed oxide 2K/Co4MnAl (labelled as 2K/Mg0 in [40]) and (ii) 2K/Co3MgMnAl mixed oxide, where Co was substituted with Mg (labelled as 2K/Mg1 in [40] or K/Co-Mg-Mn-Al in [51]).

4.2. Catalyst Characterisation and Catalytic Measurements

The catalysts were (i) characterised by atomic absorption spectroscopy (Analytic Jena AG, Jena, Germany), powder X-ray diffraction (Rigaku Corporation, Tokyo, Japan), Raman (Horiba Jobin Yvon, Longjumeau, France) and infrared spectroscopy (Thermo Fisher Scientific, Madison, WI, USA), the temperature-programmed reduction by hydrogen, the temperature-programmed desorption of CO_2 and NO, X-ray photoelectron spectroscopy, scanning electron microscopy, the work function, and N_2 physisorption and (ii) were used for the catalytic experiments of the NO decomposition.

The description of the catalyst's characterisation and catalytic experiments are described in the Supplementary Materials.

5. Conclusions

The partial substitution of cobalt in Co-Mn-Al mixed oxide for zinc and the subsequent promotion with potassium had a positive effect on the NO conversion. The potassium content was crucial for the decomposition of NO. A higher NO conversion was achieved over the samples modified by 2 wt.% K compared with the catalyst modified by 4 wt.% K. In contrast, the zinc content (7–15 wt.%) did not influence the final NO conversion. In comparison with the Mg-modified cobalt mixed oxide, the effect of the addition of Zn was lower, and the NO conversion increased in this order: non-modified < Zn-modified < Mg-modified mixed oxide catalyst. A direct correlation between the catalyst's activity and the specific surface area, basicity, the amount of desorbed NO, the amount of surface oxygen, and the temperature of the surface of the NO_x^- decomposition was found. It can be assumed that the basicity of the catalyst influenced the amount of adsorbed NO and NO_x^- species, respectively, which serve as reaction intermediates in the NO decomposition reaction. The crystallite sizes, reducibility, and work function were not the determining factors for the NO decomposition reaction. The results show that all of the physicochemical properties important for the decomposition of NO are consequences of the increased surface area with the exception of the thermal stability of the NO_x^- intermediates. Thus, we conclude that it is possible and even desirable to substitute part of cobalt with other metals to obtain a higher specific surface area and thus increase the catalytic efficiency, but simultaneously, it is necessary to ensure an optimal potassium amount, which is then closely connected with the reducibility, basicity, the amount of chemisorbed oxygen, and the stability of the NO_x^-. The dual role of K in this system points out to the different reaction steps facilitated by the basic surface sites, (i) the adsorption of the NO, and (ii) the NO decomposition.

Supplementary Materials: The following supporting information can be downloaded at: https://www.mdpi.com/article/10.3390/catal13010018/s1, Figure S1: Pore size distribution evaluated from nitrogen physical adsorption for Co-Zn-Mn-Al mixed oxide catalysts: (a) Co3ZnMnAl group of catalysts, (b) Co3.5Zn0.5MnAl group of catalysts; Figure S2: XRD patterns of catalysts precursors; Figure S3: Deconvoluted XPS spectra of (a) Co 2p; (b) Mn 2p; and (c) O 1s for different mixed oxide catalysts; Figure S4: SEM (SE) micrographs of cobalt catalysts: (a) sample 2K/Co4MnAl; (b) sample 2K/Co3MgMnAl; and (c) sample 2K/Co3ZnMnAl; Figure S5: Temperature-programmed desorption of CO_2 (TPD-CO_2) of cobalt mixed oxide catalysts without potassium; Table S1: Spinel lattice parameter a and mean coherent domain size Lc of prepared mixed oxide catalysts; Table S2: Surface concentrations of individual components of mixed oxide catalysts determined using X-ray photoelectron spectroscopy; Table S3: Turnover frequency of mixed oxide catalysts.

Author Contributions: Conceptualization, K.K. and K.P.; methodology, K.K., K.P. and L.O.; investigation, K.K., D.F., M.K., P.P. and P.S.; data curation, K.K., T.B., D.F., P.S. and M.K.; writing—original draft preparation, K.K.; writing—review and editing, K.P., L.O., M.K., P.S., T.B. and P.K.; supervision, L.O. All authors have read and agreed to the published version of the manuscript.

Funding: This research was supported by EU structural funding in Operational Programme Research, Development and Education, project No. CZ.02.1.01./0.0/0.0/17_049/0008419 "COOPERATION". Experimental results were obtained using Large Research Infrastructure ENREGAT supported by the Ministry of Education, Youth and Sports of the Czech Republic (project No. LM2018098).

Data Availability Statement: Data will be provided upon request.

Acknowledgments: We thank Alexandr Martaus, Michal Vaštyl, Eva Kinnertová, Lenka Matějová, Kamil Maciej Górecki, and Adam Hruška from the Institute of Environmental Technology, CEET, VSB–Technical University of Ostrava for the XRD, nitrogen physisorption, scanning electron microscopy, infrared spectroscopy, and AAS measurements.

Conflicts of Interest: The authors declare no conflict of interest. The funders had no role in the design of the study; in the collection, analyses, or interpretation of the data; in the writing of the manuscript; or in the decision to publish the results.

References

1. Xie, P.P.; Yong, X.; Wei, M.; Li, Y.D.; Zhang, C.J. High performance catalysts $BaCoO_3$-CeO_2 prepared by the one-pot method for NO direct decomposition. *ChemCatChem* **2020**, *12*, 4297–4303. [CrossRef]
2. Amirnazmi, A.; Benson, J.E.; Boudart, M. Oxygen inhibition in the decomposition of NO on metal oxides and platinum. *J. Catal.* **1973**, *30*, 55–65. [CrossRef]
3. Consul, J.M.D.; Peralta, C.A.; Benvenutti, E.V.; Ruiz, J.A.C.; Pastore, H.O.; Baibich, I.M. Direct decomposition of nitric oxide on alumina-modified amorphous and mesoporous silica-supported palladium catalysts. *J. Mol. Catal. A Chem.* **2006**, *246*, 33–38. [CrossRef]
4. Reddy, G.K.; Ling, C.; Peck, T.C.; Jia, H.F. Understanding the chemical state of palladium during the direct NO decomposition–influence of pretreatment environment and reaction temperature. *RSC Adv.* **2017**, *7*, 19645–19655. [CrossRef]
5. Li, Y.J.; Hall, W.K. Catalytic decomposition of nitric-oxide over Cu-zeolites. *J. Catal.* **1991**, *129*, 202–215. [CrossRef]
6. Moden, B.; Da Costa, P.; Fonfe, B.; Lee, D.K.; Iglesia, E. Kinetics and mechanism of steady-state catalytic NO decomposition reactions on Cu-ZSM5. *J. Catal.* **2002**, *209*, 75–86. [CrossRef]
7. Groothaert, M.H.; Lievens, K.; Leeman, H.; Weckhuysen, B.M.; Schoonheydt, R.A. An operando optical fiber UV-vis spectroscopic study of the catalytic decomposition of NO and N_2O over Cu-ZSM-5. *J. Catal.* **2003**, *220*, 500–512. [CrossRef]
8. Pan, K.L.; Chen, M.C.; Yu, S.J.; Yan, S.Y.; Chang, M.B. Enhancement of nitric oxide decomposition efficiency achieved with lanthanum-based perovskite-type catalyst. *J. Air Waste Manag. Assoc.* **2016**, *66*, 619–630. [CrossRef]
9. Tofan, C.; Klvana, D.; Kirchnerova, J. Decomposition of nitric oxide over perovskite oxide catalysts: Effect of CO_2, H_2O and CH_4. *Appl. Catal. B Environ.* **2002**, *36*, 311–323. [CrossRef]
10. Masui, T.; Uejima, S.; Tsujimoto, S.; Nagai, R.; Imanaka, N. Direct NO decomposition over C-type cubic Y_2O_3-Pr_6O_{11}-Eu_2O_3 solid solutions. *Catal. Today* **2015**, *242*, 338–342. [CrossRef]
11. Tsujimoto, S.; Masui, T.; Imanaka, N. Fundamental Aspects of Rare Earth Oxides Affecting Direct NO Decomposition Catalysis. *Eur. J. Inorg. Chem.* **2015**, *242*, 1524–1528. [CrossRef]
12. Sun, Q.; Wang, Z.; Wang, D.; Hong, Z.; Zhou, M.D.; Li, X.B. A review on the catalytic decomposition of NO to N_2 and O_2: Catalysts and processes. *Catal. Sci. Technol.* **2018**, *8*, 4563–4575. [CrossRef]
13. Winter, E.R.S. The catalytic decomposition of nitric oxide by metallic oxides. *J. Catal.* **1971**, *22*, 158–170. [CrossRef]
14. Park, P.W.; Kil, J.K.; Kung, H.H.; Kung, M.C. NO decomposition over sodium-promoted cobalt oxide. *Catal. Today* **1998**, *42*, 51–60. [CrossRef]
15. Haneda, M.; Kintaichi, Y.; Bion, N.; Hamada, H. Alkali metal-doped cobalt oxide catalysts for NO decomposition. *Appl. Catal. B Environ.* **2003**, *46*, 473–482. [CrossRef]
16. Peck, T.C.; Roberts, C.A.; Reddy, G.K. Contrasting effects of potassium addition on M_3O_4 (M = Co, Fe, and Mn) oxides during direct NO decomposition catalysis. *Catalysts* **2020**, *10*, 561. [CrossRef]
17. Roberts, C.A.; Paidi, V.K.; Shepit, M.; Peck, T.C.; Masias, K.L.S.; van Lierop, J.; Reddy, G.K. Effect of Cu substitution on the structure and reactivity of $Cu_xCo_{3-x}O_4$ spinel catalysts for direct NO_x decomposition. *Catal. Today* **2021**, *360*, 204–212. [CrossRef]
18. Shelef, M.; Otto, K.; Gandhi, H. Heterogeneous decomposition of nitric oxide on supported catalysts. *Atmos. Environ.* **1969**, *3*, 107–122. [CrossRef]
19. Stelmachowski, P.; Zasada, F.; Maniak, G.; Granger, P.; Inger, M.; Wilk, M.; Kotarba, A.; Sojka, Z. Optimization of multicomponent cobalt spinel catalyst for N_2O abatement from nitric acid plant tail gases: Laboratory and pilot plant studies. *Catal. Lett.* **2009**, *130*, 637–641. [CrossRef]
20. Inger, M.; Wilk, M.; Saramok, M.; Grzybek, G.; Grodzka, A.; Stelmachowski, P.; Makowski, W.; Kotarba, A.; Sojka, Z. Cobalt spinel catalyst for N_2O abatement in the pilot plant operation-long-term activity and stability in tail gases. *Ind. Eng. Chem. Res.* **2014**, *53*, 10335–10342. [CrossRef]
21. Wojcik, S.; Grzybek, G.; Stelmachowski, P.; Sojka, Z.; Kotarba, A. Bulk, surface and interface promotion of CO_3O_4 for the low-temperature N_2O decomposition catalysis. *Catalysts* **2020**, *10*, 41. [CrossRef]
22. Omata, K.; Takada, T.; Kasahara, S.; Yamada, M. Active site of substituted cobalt spinel oxide for selective oxidation of COH_2. *Appl. Catal. A Gen.* **1996**, *146*, 255–267. [CrossRef]
23. Yan, L.; Ren, T.; Wang, X.L.; Gao, Q.; Ji, D.; Suo, J.S. Excellent catalytic performance of $Zn_xCo_{1-x}Co_2O_4$ spinel catalysts for the decomposition of nitrous oxide. *Catal. Commun.* **2003**, *4*, 505–509. [CrossRef]
24. Yan, L.; Ren, T.; Wang, X.L.; Ji, D.; Suo, J.S. Catalytic decomposition of N_2O over $M_xCo_{1-x}Co_2O_4$ (M = Ni, Mg) spinel oxides. *Appl. Catal. B Environ.* **2003**, *45*, 85–90. [CrossRef]
25. Stelmachowski, P.; Maniak, G.; Kaczmarczyk, J.; Zasada, F.; Piskorz, W.; Kotarba, A.; Sojka, Z. Mg and Al substituted cobalt spinels as catalysts for low temperature deN_2O—Evidence for octahedral cobalt active sites. *Appl. Catal. B Environ.* **2014**, *146*, 105–111. [CrossRef]
26. Abu-Zied, B.M.; Obalová, L.; Pacultová, K.; Klegova, A.; Asiri, A.M. An investigation on the N_2O decomposition activity of $Mn_xCo_{1-x}Co_2O_4$ nanorods prepared by the thermal decomposition of their oxalate precursors. *J. Ind. Eng. Chem.* **2021**, *93*, 279–289. [CrossRef]
27. Abu-Zied, B.M.; Soliman, S.A.; Asiri, A.M. Role of rubidium promotion on the nitrous oxide decomposition activity of nanocrystalline Co_3O_4-CeO_2 catalyst. *Appl. Surf. Sci.* **2019**, *479*, 148–157. [CrossRef]

28. Shi, Z.B.; Yang, H.Y.; Gao, P.; Chen, X.Q.; Liu, H.J.; Zhong, L.S.; Wang, H.; Wei, W.; Sun, Y.H. Effect of alkali metals on the performance of CoCu/TiO_2 catalysts for CO_2 hydrogenation to long-chain hydrocarbons. *Chin. J. Catal.* **2018**, *39*, 1294–1302. [CrossRef]
29. Mogudi, B.M.; Ncube, P.; Bingwa, N.; Mawila, N.; Mathebula, S.; Meijboom, R. Promotion effects of alkali and alkaline earth metals on catalytic activity of mesoporous Co_3O_4 for 4-nitrophenol reduction. *Appl. Catal. B Environ.* **2017**, *218*, 240–248. [CrossRef]
30. Li, Z.J.; Zhong, L.S.; Yu, F.; An, Y.L.; Dai, Y.Y.; Yang, Y.Z.; Lin, T.J.; Li, S.G.; Wang, H.; Gao, P.; et al. Effects of sodium on the catalytic performance of CoMn catalysts for fischer-tropsch to olefin reactions. *ACS Catal.* **2017**, *7*, 3622–3631. [CrossRef]
31. Maniak, G.; Stelmachowski, P.; Kotarba, A.; Sojka, Z.; Rico-Perez, V.; Bueno-Lopez, A. Rationales for the selection of the best precursor for potassium doping of cobalt spinel based deN_2O catalyst. *Appl. Catal. B Environ.* **2013**, *136*, 302–307. [CrossRef]
32. Pacultová, K.; Draštíková, V.; Chromčáková, Ž.; Bílková, T.; Kutláková, K.M.; Kotarba, A.; Obalová, L. On the stability of alkali metal promoters in Co mixed oxides during direct NO catalytic decomposition. *Mol. Catal.* **2017**, *428*, 33–40. [CrossRef]
33. Bílková, T.; Fridrichová, D.; Pacultová, K.; Karásková, K.; Obalová, L.; Haneda, M. Reaction mechanism of NO direct decomposition over K-promoted Co-Mn-Al mixed oxides-DRIFTS, TPD and transient state studies. *J. Taiwan Inst. Chem. Eng.* **2021**, *120*, 257–266. [CrossRef]
34. Grzybek, G.; Wójcik, S.; Legutko, P.; Gryboś, J.; Indyka, P.; Leszczyński, B.; Kotarba, A.; Sojka, Z. Thermal stability and repartition of potassium promoter between the support and active phase in the K-$Co_{2.6}Zn_{0.4}O_4$ | α-Al_2O_3 catalyst for N_2O decomposition: Crucial role of activation temperature on catalytic performance. *Appl. Catal. B Environ.* **2017**, *205*, 597–604. [CrossRef]
35. Kovanda, F.; Rojka, T.; Dobešová, J.; Machovič, V.; Bezdička, P.; Obalová, L.; Jirátová, K.; Grygar, T. Mixed oxides obtained from Co and Mn containing layered double hydroxides: Preparation, characterization, and catalytic properties. *J. Solid State Chem.* **2006**, *179*, 812–823. [CrossRef]
36. An, H.; McGinn, P.J. Catalytic behavior of potassium containing compounds for diesel soot combustion. *Appl. Catal. B Environ.* **2006**, *62*, 46–56. [CrossRef]
37. Pacultová, K.; Bílková, T.; Klegova, A.; Karásková, K.; Fridrichová, D.; Jirátová, K.; Kiška, T.; Balabánová, J.; Koštejn, M.; Kotarba, A.; et al. Co-Mn-Al mixed oxides promoted by K for direct NO decomposition: Effect of preparation parameters. *Catalysts* **2019**, *9*, 593. [CrossRef]
38. Jirátová, K.; Pacultová, K.; Balabánová, J.; Karásková, K.; Klegova, A.; Bílková, T.; Jandová, V.; Koštejn, M.; Martaus, A.; Kotarba, A.; et al. Precipitated K-promoted Co-Mn-Al mixed oxides for direct no decomposition: Preparation and properties. *Catalysts* **2019**, *9*, 592. [CrossRef]
39. Jirátová, K.; Pacultová, K.; Karásková, K.; Balabánová, J.; Koštejn, M.; Obalová, L. Direct Decomposition of NO over Co-Mn-Al Mixed Oxides: Effect of Ce and/or K Promoters. *Catalysts* **2020**, *10*, 808. [CrossRef]
40. Karásková, K.; Pacultová, K.; Klegova, A.; Fridrichová, D.; Valašková, M.; Jirátová, K.; Stelmachowski, P.; Kotarba, A.; Obalová, L. Magnesium Effect in K/Co-Mg-Mn-Al Mixed Oxide Catalyst for Direct NO Decomposition. *Catalysts* **2020**, *10*, 931. [CrossRef]
41. Bomfim, H.E.L.; Oliveira, A.C.; Rangel, M.d.C. Effect of zinc on the catalytic activity of hematite in ethylbenzene dehydrogenation. *React. Kinet. Catal. Lett.* **2003**, *80*, 359–364. [CrossRef]
42. Tatarchuk, T.; Paliychuk, N.; Pacia, M.; Kaspera, W.; Macyk, W.; Kotarba, A.; Bogacz, B.F.; Pedziwiatr, A.T.; Mironyuk, I.; Gargula, R.; et al. Structure-redox reactivity relationships in $Co_{1-x}Zn_xFe_2O_4$: The role of stoichiometry. *N. J. Chem.* **2019**, *43*, 3038–3049. [CrossRef]
43. Tiwari, P.; Verma, R.; Kane, S.N.; Tatarchuk, T.; Mazaleyrat, F. Effect of Zn addition on structural, magnetic properties and anti-structural modeling of magnesium-nickel nano ferrites. *Mater. Chem. Phys.* **2019**, *229*, 78–86. [CrossRef]
44. Russo, N.; Fino, D.; Saracco, G.; Specchia, V. N_2O catalytic decomposition over various spinel-type oxides. *Catal. Today* **2007**, *119*, 228–232. [CrossRef]
45. Obalová, L.; Karásková, K.; Jirátová, K.; Kovanda, F. Effect of potassium in calcined Co-Mn-Al layered double hydroxide on the catalytic decomposition of N_2O. *Appl. Catal. B Environ.* **2009**, *90*, 132–140. [CrossRef]
46. Legutko, P.; Jakubek, T.; Kaspera, W.; Stelmachowski, P.; Sojka, Z.; Kotarba, A. Soot oxidation over K-doped manganese and iron spinels–How potassium precursor nature and doping level change the catalyst activity. *Catal. Commun.* **2014**, *43*, 34–37. [CrossRef]
47. Jiratova, K.; Mikulova, J.; Klempa, J.; Grygar, T.; Bastl, Z.; Kovanda, F. Modification of Co-Mn-Al mixed oxide with potassium and its effect on deep oxidation of VOC. *Appl. Catal. A Gen.* **2009**, *361*, 106–116. [CrossRef]
48. Klyushina, A.; Pacultová, K.; Karásková, K.; Jirátová, K.; Ritz, M.; Fridrichová, D.; Volodarskaja, A.; Obalová, L. Effect of preparation method on catalytic properties of Co-Mn-Al mixed oxides for N_2O decomposition. *J. Mol. Catal. A Chem.* **2016**, *425*, 237–247. [CrossRef]
49. Zasada, F.; Piskorz, W.; Sojka, Z. Cobalt spinel at various redox conditions: DFT+U investigations into the structure and surface thermodynamics of the (100) facet. *J. Phys. Chem. C* **2015**, *119*, 19180–19191. [CrossRef]
50. Jakubek, T.; Kaspera, W.; Legutko, P.; Stelmachowski, P.; Kotarba, A. Surface versus bulk alkali promotion of cobalt-oxide catalyst in soot oxidation. *Catal. Commun.* **2015**, *71*, 37–41. [CrossRef]
51. Pacultová, K.; Klegova, A.; Karásková, K.; Fridrichová, D.; Bílková, T.; Koštejn, M.; Obalová, L. Oxygen effect in NO direct decomposition over K/Co-Mg-Mn-Al mixed oxide catalyst–Temperature programmed desorption study. *Mol. Catal.* **2021**, *510*, 111695. [CrossRef]

52. Biesinger, M.C.; Payne, B.P.; Grosvenor, A.P.; Lau, L.W.M.; Gerson, A.R.; Smart, R.S. Resolving surface chemical states in XPS analysis of first row transition metals, oxides and hydroxides: Cr, Mn, Fe, Co and Ni. *Appl. Surf. Sci.* **2011**, *257*, 2717–2730. [CrossRef]
53. Obalová, L.; Karásková, K.; Wach, A.; Kustrowski, P.; Mamulová-Kutláková, K.; Michalik, S.; Jirátová, K. Alkali metals as promoters in Co-Mn-Al mixed oxide for N_2O decomposition. *Appl. Catal. A-Gen.* **2013**, *462*, 227–235. [CrossRef]
54. Chromčáková, Ž.; Obalová, L.; Kovanda, F.; Legut, D.; Titov, A.; Ritz, M.; Fridrichová, D.; Michalik, S.; Kuśtrowski, P.; Jirátová, K. Effect of precursor synthesis on catalytic activity of Co_3O_4 in N_2O decomposition. *Catal. Today* **2015**, *257*, 18–25. [CrossRef]
55. Karásková, K.; Pacultová, K.; Jirátová, K.; Fridrichová, D.; Koštejn, M.; Obalová, L. K-Modified Co-Mn-Al Mixed Oxide-Effect of Calcination Temperature on N_2O Conversion in the Presence of H_2O and NO_x. *Catalysts* **2020**, *10*, 1134. [CrossRef]
56. Langell, M.A.; Gevrey, F.; Nydegger, M.W. Surface composition of $Mn_xCo_{1-x}O$ solid solutions by X-ray photoelectron and Auger spectroscopies. *Appl. Surf. Sci.* **2000**, *153*, 114–127. [CrossRef]
57. Kim, S.C.; Shim, W.G. Catalytic combustion of VOCs over a series of manganese oxide catalysts. *Appl. Catal. B Environ.* **2010**, *98*, 180–185. [CrossRef]
58. Obalová, L.; Pacultová, K.; Balabánová, J.; Jirátová, K.; Bastl, Z.; Valášková, M.; Lacný, Z.; Kovanda, F. Effect of Mn/Al ratio in Co–Mn–Al mixed oxide catalysts prepared from hydrotalcite-like precursors on catalytic decomposition of N_2O. *Catal. Today* **2007**, *119*, 233–238. [CrossRef]
59. Moulder, J.F.; Stickle, W.F.; Sobol, P.E.; Bomben, K.D. *Handbook of X-ray Photoeletron Spectroscopy: A Reference Book of Standard Spectra for Identification and Interpretation of XPS Data*; Perkin-Elmer Corporation: Eden Prairie, MN, USA, 1995.
60. Dupin, J.C.; Gonbeau, D.; Vinatier, P.; Levasseur, A. Systematic XPS studies of metal oxides, hydroxides and peroxides. *Phys. Chem. Chem. Phys.* **2000**, *2*, 1319–1324. [CrossRef]
61. Piumetti, M.; Bensaid, S.; Russo, N.; Fino, D. Nanostructured ceria-based catalysts for soot combustion: Investigations on the surface sensitivity. *Appl. Catal. B Environ.* **2015**, *165*, 742–751. [CrossRef]
62. Chuang, T.J.; Brundle, C.R.; Rice, D.W. Interpretation of X-ray photoemission spectra of cobalt oxides and cobalt oxide surfaces. *Surf. Sci.* **1976**, *59*, 413–429. [CrossRef]
63. Pacultová, K.; Karásková, K.; Kovanda, F.; Jirátová, K.; Šramek, J.; Kustrowski, P.; Kotarba, A.; Chromčáková, Ž.; Kočí, K.; Obalová, L. K-doped Co-Mn-Al mixed oxide catalyst for N_2O abatement from nitric acid plant waste gases: Pilot plant studies. *Ind. Eng. Chem. Res.* **2016**, *55*, 7076–7084. [CrossRef]
64. Kannan, S.; Swamy, C.S. Catalytic decomposition of nitrous oxide over calcined cobalt aluminum hydrotalcites. *Catal. Today* **1999**, *53*, 725–737. [CrossRef]
65. Chen, H.H.; Yang, M.; Tao, S.; Chen, G.W. Oxygen vacancy enhanced catalytic activity of reduced Co_3O_4 towards p-nitrophenol reduction. *Appl. Catal. B Environ.* **2017**, *209*, 648–656. [CrossRef]
66. Luo, Y.J.; Zheng, Y.B.; Zuo, J.C.; Feng, X.S.; Wang, X.Y.; Zhang, T.H.; Zhang, K.; Jiang, L.L. Insights into the high performance of Mn-Co oxides derived from metal organic frameworks for total toluene oxidation. *J. Hazard. Mater.* **2018**, *349*, 119–127. [CrossRef]
67. Wang, Z.P.; Zhang, X.M.; Wang, L.G.; Zhang, Z.L.; Jiang, Z.; Xiao, T.C.; Umar, A.; Wang, Q. Co-Mn-Al nonstoichiometric spinel-type catalysts derived from hydrotalcites for the simultaneous removal of soot and nitrogen oxides. *Sci. Adv. Mater.* **2013**, *5*, 1449–1457. [CrossRef]
68. Imanaka, N.; Masui, T. Advances in direct NO_x decomposition catalysts. *Appl. Catal. A Gen.* **2012**, *431–432*, 1–8. [CrossRef]
69. Haneda, M.; Hamada, H. Recent progress in catalytic NO decomposition. *Comptes Rendus Chim.* **2016**, *19*, 1254–1265. [CrossRef]
70. Hong, W.-J.; Iwamoto, S.; Inoue, M. Direct NO decomposition over a Ce–Mn mixed oxide modified with alkali and alkaline earth species and CO_2-TPD behavior of the catalysts. *Catal. Today* **2011**, *164*, 489–494. [CrossRef]
71. Haneda, M.; Kintaichi, Y.; Hamada, H. Reaction mechanism of NO decomposition over alkali metal-doped cobalt oxide catalysts. *Appl. Catal. B Environ.* **2005**, *55*, 169–175. [CrossRef]
72. Ishihara, T.; Ando, M.; Sada, K.; Takiishi, K.; Yamada, K.; Nishiguchi, H.; Takita, Y. Direct decomposition of NO into N_2 and O_2 over La(Ba)Mn(In)O_3 perovskite oxide. *J. Catal.* **2003**, *220*, 104–114. [CrossRef]
73. Zhu, J.; Xiao, D.; Li, J.; Xie, X.; Yang, X.; Wu, Y. Recycle—New possible mechanism of NO decomposition over perovskite(-like) oxides. *J. Mol. Catal. A Chem.* **2005**, *233*, 29–34. [CrossRef]
74. Obalová, L.; Maniak, G.; Karásková, K.; Kovanda, F.; Kotarba, A. Electronic nature of potassium promotion effect in Co-Mn-Al mixed oxide on the catalytic decomposition of N_2O. *Catal. Commun.* **2011**, *12*, 1055–1058. [CrossRef]
75. Obalová, L.; Jirátová, K.; Kovanda, F.; Valášková, M.; Balabánová, J.; Pacultová, K. Structure–activity relationship in the N_2O decomposition over Ni-(Mg)-Al and Ni-(Mg)-Mn mixed oxides prepared from hydrotalcite-like precursors. *J. Mol. Catal. A Chem.* **2006**, *248*, 210–219. [CrossRef]

Disclaimer/Publisher's Note: The statements, opinions and data contained in all publications are solely those of the individual author(s) and contributor(s) and not of MDPI and/or the editor(s). MDPI and/or the editor(s) disclaim responsibility for any injury to people or property resulting from any ideas, methods, instructions or products referred to in the content.